Wood Sci Technol (2004) 38: 641–659
DOI 10.1007/s00226-004-0253-5

ORIGINAL

Kristian Krabbenhoft · Lars Damkilde

Double porosity models for the description of water infiltration in wood

Received: 10 November 2003 / Published online: 13 November 2004

Abstract In this paper some of the possibilities of applying double porosity and permeability models to the problem of water infiltration in wood are explored. It is shown that the double porosity model can capture a number of commonly reported anomalies including two-stage infiltration/sorption and apparent sample length dependent transfer parameters. Starting with the double porosity model, several extensions are discussed and the type of principal behaviour possible with the models is elaborated on. Finally, a set of highly anomalous experimental results is fitted to within a reasonable accuracy by a double permeability model.

List of symbols

P	Pressure, Pa
X	Water content (dry porous material basis)
$\mathbf{v}$	Velocity, m s^{-1}
K	Absolute/relative permeability
D, D	Diffusivity, m^2 s^{-1} or kg m^{-1} s^{-1} Pa^{-1}
M	Molar mass, kg mol^{-1}
R	Ideal gas constant, J mol^{-1} K^{-1}
T	Temperature, K

Greek symbols

ρ	Concentration/density, kg m^{-3}
μ	Viscosity, kg m^{-1} s^{-1}
ϕ	Porosity
ε	Volume fraction

K. Krabbenhoft
Department of Civil Engineering, Technical University of Denmark,
Lyngby, Denmark

L. Damkilde
Institute of Chemistry and Applied Engineering Science, Aalborg University Esbjerg,
Esbjerg, Denmark

Present address: K. Krabbenhoft (✉)
Department of Civil, Surveying and Environmental Engineering,
University of Newcastle, NSW, 2300, Australia
E-mail: kristian.krabbenhoft@newcastle.edu.au

Subscripts

w	Water
f	Free water
v	Water vapour
g	Gas—water vapour + dry air
b	Bound water
c	Capillary
s	Solid skeleton
r	Relative
FSP	Fiber saturation point
surf	External exchange surface

Mathematical symbols

$\bar{\cdot}$	Averaging operator
$\nabla\cdot$	Divergence operator
∇	Gradient operator

Introduction

The transport of water in wood is an important problem for a number of reasons. Since wood is a material whose mechanical properties are strongly dependent on its moisture content and moisture content history, it is important to be able to assess the influence of the interaction of wooden structures with the surrounding environment. Furthermore, green lumber must be dried before it is used as structural timber, and since this process is both expensive as well as critical for the quality of the end product it is useful to be able to predict the temporal variations of moisture content and temperature during drying. Another problem in which the transport of water is important is in the treatment of wood with artificial preservatives. Traditionally, the bulk of the theoretical and numerical models have been concerned with the problem of drying, i.e. the removal of water, whereas much less work has been done in relation to the reverse problem of infiltration. This problem finds application in preservation processing and in connection with environmental loads such as rain and snow as well as for timber structures partially embedded in soil (Krabbenhoft et al. 2003).

The most complete transport models, such as those treated in Spolek et al. (1985), Ouelhazi et al. (1992), Couture et al. (1996), and Perre and Turner (1999), are based on the classical averaging theorems for porous media flow (see e.g. Whitaker 1977) by which the transport of heat and mass are described by a set of coupled partial differential equations, which make reference to a macroscopic scale rather than the microscopic scale at which the flow through tracheids, pits, and so on, could be considered. This approach is also widely accepted and applied for the transport of heat and mass in a number of other porous materials, most notably soils (see e.g. Lewis and Schrefler 2000). In recent years, however, it has been realized that flow of water in soils is significantly influenced by the presence of heterogeneities such as fractures,

fissures, cracks and macropores (Mortensen 2001; Haria et al. 2003). The flow patterns induced by these heterogeneities cannot be adequately described in the framework of the classical averaging models. On the other hand, although in principle possible, it is not practically feasible to consider the exact nature of the porous medium and include all heterogeneities into the model. Therefore, models have been developed which maintain the overall macroscopic view but which make reference to two or more interacting zones with widely different flow properties. If two zones, commonly referred to as fracture and matrix, are considered the corresponding models are referred to as double porosity or double permeability models depending on whether flow takes place in both zones or only in one (Fig. 1). In Fig. 1a the conventional macroscopic single continuum model is shown. Here no distinction is made between fracture and matrix zones. However, the material parameters may vary throughout the domain as indicated by the three different subdomains FM1–FM3. In the case of wood, a board containing both heartwood and sapwood could possibly be treated by the single continuum model, namely by using two different sets of material parameters for the two different types of wood. In Fig. 1b the double porosity model is shown which considers separately the fracture and matrix zones. As illustrated, flow occurs only in the fracture zone whereas the matrix acts as a reservoir which can only store and exchange water with the fracture zone. As a generalization of this model, the double permeability model shown in Fig. 1c considers flow in both the fracture as well as the matrix zone. Thus, the double porosity model appears as a special case of the double permeability model, whereas the single continuum model is contained as a special case in both the double porosity and the double permeability model.

In the drying of wood, good agreement between theory and experiment has generally been found (Spolek et al. 1985; Ouelhazi et al. 1992; Couture et al. 1996; Perre 1987; Pang 1998; Goyeneche et al. 2002); although, several issues, including the description of the flow at low degrees of free water saturation (Couture et al. 1996; Goyeneche et al. 2002), remain somewhat controversial. In infiltration, however, agreement between theory and experiment seems to be much more difficult to attain. Of course, the general set of governing equations

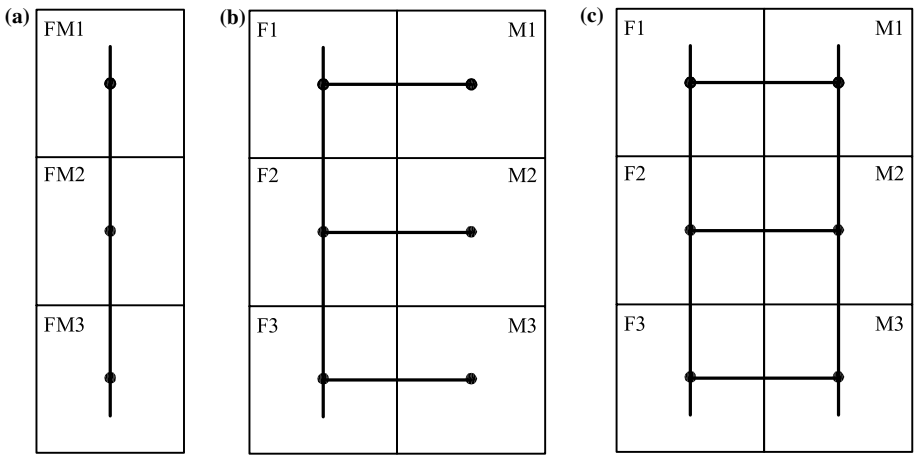

Fig. 1 Transport models: single continuum model (**a**), double-porosity model (**b**), and double-permeability model (**c**). Adapted from Mortensen (2001)

applied in the case of drying are, in principle, also valid in the case of infiltration. However, the rate of drying is often to a large degree governed by the rate of evaporation at the exchange surface, which is relatively easy to quantify, rather than by the internal transfer. In infiltration, on the other hand, the entire process is governed solely by the internal transfer properties, which may be very difficult to quantify in terms of the single continuum model. Indeed, Banks (1981) goes as far as to speculate that [no tag]the precise prediction of liquid penetration rate from steady state permeability data may be illusory'. An example of some of the difficulties encountered is contained in a recent one dimensional infiltration experiment on beech (Perre 1998). Here the theory predicted a time scale in the order of minutes whereas the actual time scale turned out to be in the order of days or weeks. Moreover, the moisture profiles measured seemed to be in very poor agreement with what one would expect on the basis of a single continuum model.

As was suggested in Perre (1998) the observed behaviour is probably due to the structure of the wood. In Fig. 2 the cellular structure of a so-called diffuse porous hardwood, to which category beech belongs, is shown. Looking at this figure it is not hard to conceive that the transport of water of a one dimensional longitudinal sample would be primarily by way of the large vessels with a simultaneous, but much slower infiltration into the denser material surrounding the vessels. This type of transfer corresponds quite closely to what can be represented by the double porosity model illustrated in Fig. 1b. This model thus seems to be a natural extension of the conventional macroscopic model.

This mode of transfer could also be important in other species of wood. In ring porous hardwoods, Fig. 3a, the situation is the same, i.e. large vessels and surrounding dense material. In softwoods, Fig. 3b, it is well-known (see e.g. Siau 1984), that infiltration into dry wood is more rapid in the latewood than in the earlywood, and that the ratio between the transfer rates is greater in the sapwood than in the heartwood. This is perhaps somewhat contrary to what should be expected since in the green state the thinwalled earlywood is much more permeable than the latewood. However, during drying the pits which connect the individual cells, and thus provide the principal pathways for water flow, have a much higher tendency to blocking up in the earlywood than in the latewood.

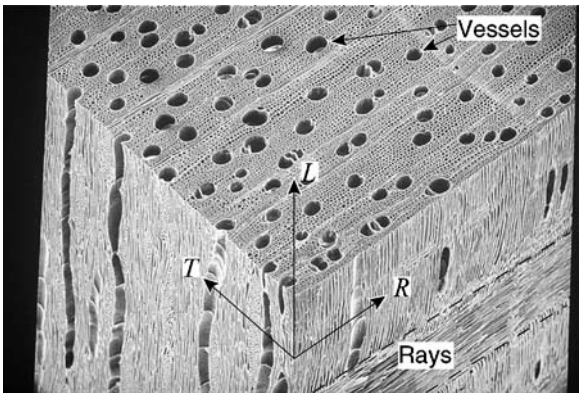

Fig. 2 Microscopic structure of a diffuse porous hardwood (sugar sample) (Structure of Wood 2003)

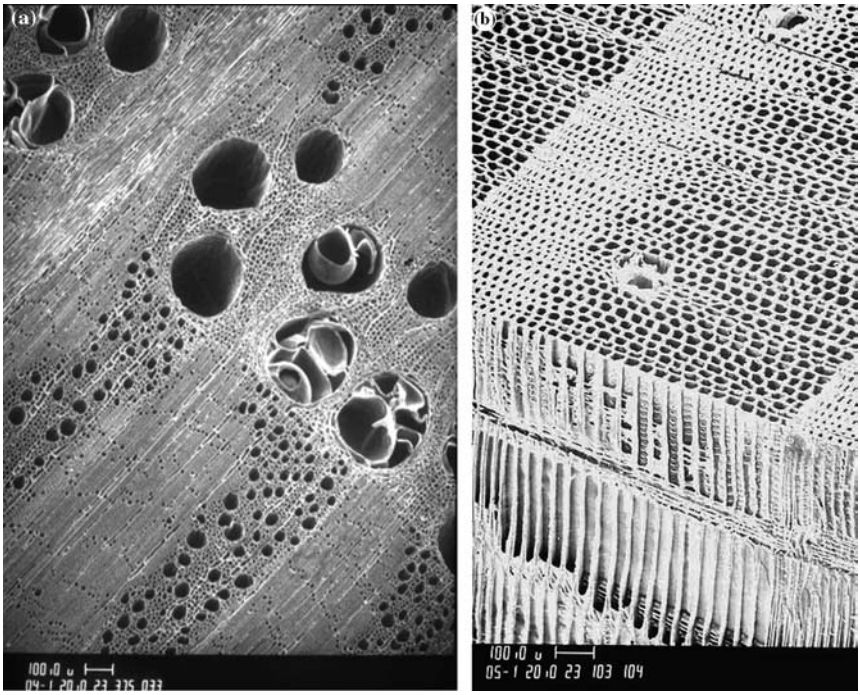

Fig. 3 Microscopic structure of ring-porous hardwood (*white oak*) (**a**), and softwood (*Douglas fir*) (**b**) (Structure of Wood 2003)

Whereas the applicability of the double porosity model seems very plausible for infiltration in the longitudinal direction, there seems to be less justification for using the approach to flow in the other two directions. However, in the radial direction, the presence of ray cells (Fig. 2) constitutes a possible rapid route for water transport, again with a simultaneous infiltration into the denser material surrounding the rays cells. In the tangential direction, the flow of water must necessarily be exclusively by way of the pits connecting the cells. In this direction no macropores are thus present. It seems, therefore, that for general three dimensional conditions, the double porosity model does not suffice. That is, the flow in the [no tag]matrix', especially in the tangential direction, is too significant to be ignored, and for this reason the double permeability model rather than the double porosity model should be considered in the general three dimensional case.

As for other porous materials the applicability of double porosity/permeability model could also be expected. In cement paste, for example, the problems with applying single continuum models for the infiltration of water is well documented (see e.g. Martys and Ferraris 1997; Krus et al. 1997). Similarly, in cellular concrete very poor agreement between theory and experiment has been reported (Nielsen 1974; Hansen 1993). Recently, a number of different porous materials, including fired-clay brick and sandstone, were all shown to exhibit a behaviour during infiltration which does not comply with the common theory (Kuntz and Lavallee 2001). The application of double porosity/permeability models to these materials could be justified on the basis of the pore size distribution, i.e. with water being transferred quite rapidly in the larger pores with a simultaneous infiltration into the smaller pores, similar to what is the case in

soils. Although there may well be other mechanisms involved, the double porosity/permeability models seem to be worth considering, at least because of their very clear physical interpretation.

In the following the conventional macroscopic single continuum model is briefly discussed after which several double porosity and permeability models are presented. Throughout, numerical examples demonstrating the differences between the single continuum and the double porosity/permeability model are given. Finally, the numerical solution of the various models by the finite element method is discussed.

Single continuum model

The single continuum model considers the conservation of the three water phases as well as dry atmospheric air and enthalpy. For reasons of simplicity we will assume isothermal and atmospheric conditions throughout. The relevant conservation equations are then

$$\begin{array}{lll} \text{Free water:} & \frac{\partial}{\partial t}(\varepsilon_w \rho_w) & +\nabla \cdot (\rho_w \mathbf{v}_w) = -\dot{m}_{wv} - \dot{m}_{wb} \\ \text{Bound water:} & \frac{\partial}{\partial t}(\varepsilon_s \rho_b) & +\nabla \cdot (\rho_b \mathbf{v}_b) = -\dot{m}_{bv} - \dot{m}_{wb} \\ \text{Water vapour:} & \frac{\partial}{\partial t}(\varepsilon_g \rho_v) & +\nabla \cdot (\rho_v \mathbf{v}_v) = \dot{m}_{wv} + \dot{m}_{bv} \end{array} \quad (1)$$

where ε_w, ε_s, ε_g are the volume fractions of free water, solid skeleton and gas (vapour and air) phases, and ρ_w, ρ_b and ρ_w are the corresponding concentrations of free water, bound water and water vapour. The mass average velocities of the different water phases are given by $\mathbf{v}_w$, $\mathbf{v}_b$ and $\mathbf{v}_v$. These equations are quite general and also include the transition of one phase to another, i.e. $\dot{m}_{wv}$ describes the rate of conversion of free water to bound water, $\dot{m}_{bv}$ the conversion of bound water to water vapour, and $\dot{m}_{wb}$ accounts for the conversion of bound water to free water and vice versa. Recently, it has been shown (Krabbenhoft and Damkilde 2003) that the non-equilibrium between water vapour and bound water is a key ingredient in accurately describing moisture transfer in the hygroscopic range. In this way the flow phenomena often referred to as [no tag]non-Fickian' (Wadsö 1994) can be accurately described. Nevertheless, in the interest of simplicity and because the primary focus is on the conditions above the fiber saturation point, we will assume equilibrium between all water phases as is usually done. The three conservation equations of Eqs. 1 can then be reduced to one describing the conservation of the total water

$$\text{Total water}: \quad \frac{\partial \theta}{\partial t} + \nabla \cdot (\rho_w \mathbf{v}_w + \rho_b \mathbf{v}_b + \rho_v \mathbf{v}_v) = 0 \quad (2)$$

where θ is the total water content (kg m^{-3}). Since wood is a highly hygroscopic material it is necessary to separate this total moisture content into bound water and free water

$$\theta = \theta_f + \theta_b \quad (3)$$

where the bound water content is defined as

$$\theta_b = \min(\theta, \rho_0 M_{FSP}) \quad (4)$$

with M_{FSP} being the dry base moisture content at the fiber saturation point and ρ_0 the dry density. Next, the conservation Eq. 2 must be supplemented with

appropriate constitutive relations. For the free water phase Darcy's law is applied

$$\rho_w \mathbf{v}_w = -\rho_w \frac{KK_r}{\mu_w} \nabla(p_w + \rho_w g z) \tag{5}$$

where K is the absolute permeability, K_r the relative permeability which depends on fluid saturation, μ_w the dynamic viscosity of water, and p_w the water pressure which under partially saturated and atmospheric conditions is equivalent to the capillary pressure p_c. Gravity is defined as acting opposite to the z-coordinate.

The bound water flux is described by a gradient law with the bound water moisture content as driving force (Siau 1984)

$$\rho_b \mathbf{v}_b = \mathrm{D}_b \nabla \theta_b \tag{6}$$

For the vapour flux convective transfer is ignored and Fick's law used to describe the diffusive flux. Under isothermal conditions this can be written as

$$\rho_v \mathbf{v}_v = \frac{M_w}{RT} \mathrm{D}_v \nabla p_v \tag{7}$$

where D_v is the effective water vapour diffusivity.

Thus, the full equation describing the transfer of water vapour, bound water and free water is given by

$$\frac{\partial \theta}{\partial t} = \nabla \cdot \left[\rho_w \frac{KK_r}{\mu_w} \nabla(p_w + \rho_w g z) + \mathrm{D}_b \nabla \theta_b + \frac{M_w}{RT} \mathrm{D}_v \nabla p_v \right] \tag{8}$$

The total water conservation Eq. 8 requires a significant number of material parameters which in principle can be determined in a number of independent experiments. In infiltration the far largest contribution to the total water flux is that of free water. To describe the transfer of this component the absolute and relative permeabilities as well as the capillary pressure-saturation curve must be determined. Such relations are available for green wood, although they are subject to a large degree of uncertainty and must generally be used with some caution (Couture et al. 1996; Goyeneche et al. 2002). For wood which has been dried, however, we do not know of any complete set of relations. Therefore, in the following, we will use a transport equation which does not explicitly involve these relations. If we assume partially saturated conditions and neglect gravity then Eq. 8 can be written in terms of θ only as

$$\frac{\partial \theta}{\partial t} = \nabla \cdot (\mathrm{D}_\theta \nabla \theta) \tag{9}$$

where the effective total water diffusivity is given by

$$D_\theta = \rho_w \frac{KK_r}{\mu_w} \left(\frac{\partial p_c}{\partial \theta} \right) + \mathrm{D}_b \left(\frac{\partial \theta_b}{\partial \theta} \right) + \frac{M_w}{RT} \mathrm{D}_v \left(\frac{\partial p_v}{\partial \theta} \right) \tag{10}$$

Thus, instead of measuring each of the components in Eq. 10 in a number of independent experiments, there is also the possibility of measuring the effective diffusivity D_θ directly in a single experiment. This approach has been taken to wood in Tremblay et al. (2000) and Signe Kamp (2003), and in Pel (1995) to a number of other porous building materials. Thus, in the following we will make

reference to Eq. 9 rather than to Eq. 8 and assume the effective diffusivity given as function of the total water content.

It should be borne in mind that this approach is far from ideal. First of all, gravity is neglected, which in many applications may be quite erroneous. Furthermore, there is no real possibility of taking externally applied water pressures greater than the maximum capillary pressure into account. As a first approximation, however, the approach is acceptable although in the future the consistent Darcian model in Eq. 8 should be preferred.

Properties of the infiltration equation and reported anomalies

The governing equation (Eq. 9) belongs to the class of nonlinear diffusion problems which are treated extensively, e.g. in Crank (1967). Although usually very hard to solve analytically, quite a lot of information about the principal behaviour of the these equations can be extracted. Since the effective diffusivity is usually a very strong function of the moisture content, often increasing over several decades from the dry to the fully saturated state, a shock-like behaviour is often seen when tracking the moisture content profiles in time. This is shown in Fig. 4a, where a one dimensional infiltration in the longitudinal direction of a 5-cm softwood sample has been simulated using standard material parameters (Perré and Turner 1999). For such experiments the fractional weight increase as a function the square root of time is often plotted and a curve similar to the one shown in Fig. 4b should then result. That is, the curve should be linear up the point where the front reaches the dry end of the sample. One of the most cited anomalies is deviations from this curve, and these are often of the form of a two-stage infiltration as reported by Martys and Ferraris (1997), Nielsen (1974), and Hansen (1993). That is, the fractional weight increase curve indicates a rapid initial sorption of a certain amount of water, followed by a much slower sorption which proceeds until full saturation.

In Fig. 5a the moisture content profiles resulting from infiltration into a sample of beech are shown. As can be seen the moisture content increases rapidly near the wet end, whereas the subsequent infiltration is very slow. This is clearly seen from the fractional weight increase curve in Fig. 5b which is not at all as should be expected. The explanation given in Perre (1998) for this behaviour is that a portion of the water is carried very rapidly in the vessels with

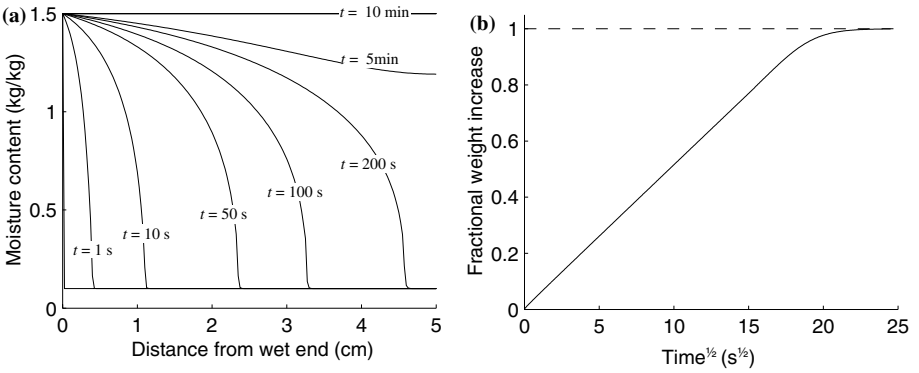

Fig. 4 One dimensional single continuum model infiltration

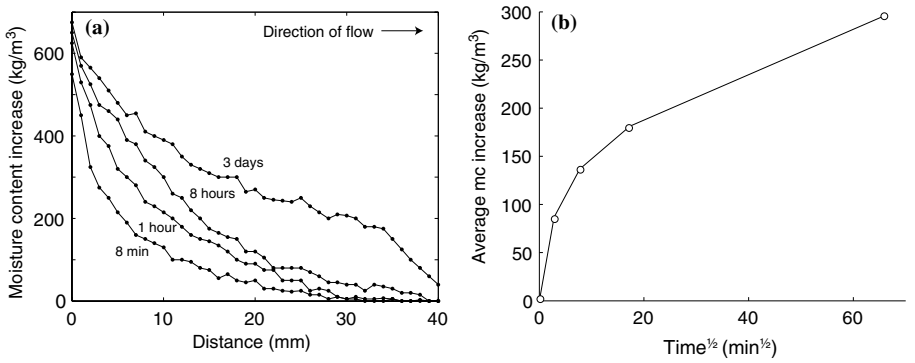

Fig. 5 Infiltration in beech (Perre 1998)

a simultaneous, but much slower, infiltration into the denser material surrounding the vessel. Another example of an anomalous infiltration in wood is shown in Fig. 6 where the material is fir sapwood. These moisture content profiles are particularly interesting in that they clearly reveal both the propagation of a front as well as a simultaneous slow absorption.

Clearly, the behaviour encountered in these two experiments cannot be simulated using the standard single continuum model. As previously mentioned, similar anomalies have been reported for a number of other porous materials. Recently, Kuntz and Lavallee (2001) proposed that instead of using the standard diffusion Eq. 9 the moisture flux should be taken as

$$j = -D(\theta)\left(\frac{\partial\theta}{\partial z}\right)^n \tag{11}$$

such that the governing equation would be

$$\frac{\partial\theta}{\partial t} = \frac{\partial}{\partial z}\left[D(\theta)\left(\frac{\partial\theta}{\partial z}\right)^n\right] \tag{12}$$

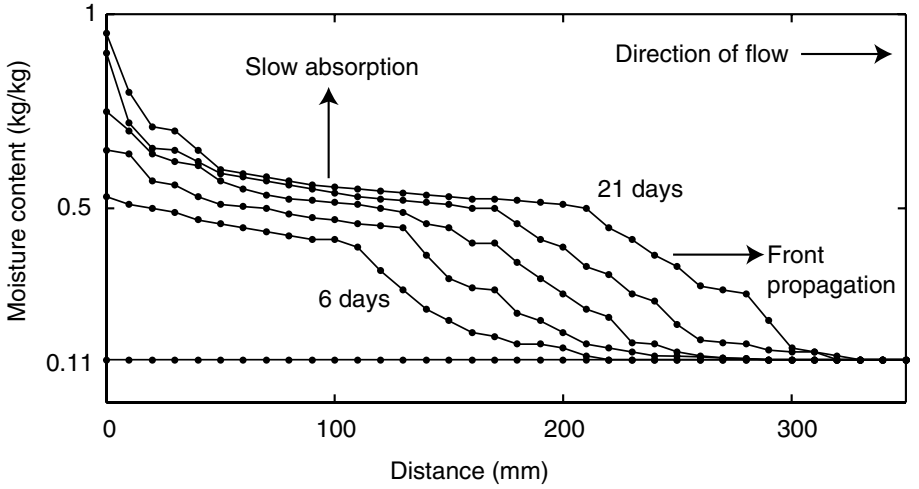

Fig. 6 Infiltration in fir sapwood (K.K. Hansen and J.B. Jensen, unpublished data)

where n is not necessarily equal to unity. This gives fractional weight increase curves which are linear when plotted as a function of $t^{1/(n+1)}$. Although such an expression for the flux cannot be ruled out, the underlying physics of the modified gradient law is somewhat unclear. Nevertheless, a number of infiltration experiments involving non-organic porous materials were fitted quite well.

Another recent proposition involves a time dependent diffusion coefficient. Thus, Lockington and Parlange (2003) argue that in cement based materials where there is the possibility of some chemo-mechanical interaction, a governing equation of the type

$$\frac{\partial\theta}{\partial t} = \frac{\partial}{\partial z}\left(\gamma(t)\delta(\theta)\frac{\partial\theta}{\partial z}\right) \tag{13}$$

should be considered. For wood, such a time dependent diffusion coefficient could be argued since in wood there is a swelling and a subsequent relaxation upon exposure to moisture. Moreover, the validity of using such a time dependent diffusion coefficient can easily be proved or disproved by initiating the experiment from conditions closer or further from the fiber saturation point, below which all moisture–mechanical interaction takes place.

In the following, an alternative explanation for the anomalies encountered is sought in terms of the double porosity/permeability models. We focus on the different principal behaviours which can be simulated using these models. Furthermore, an attempt to explain a set of experimental results in terms of the models is made.

Since no analytic solutions are available for the coupled nonlinear diffusion equations which define the models, all computations are done numerically by the finite element method as described in Appendix.

Double porosity and permeability models

In the following, the double porosity and permeability models are presented and some of their properties described.

The total moisture content is separated into two contributions α and β with the parameter η describing the volume fraction of the α-zone. Thus, the total moisture content is given by a weighted sum as

$$\theta = \eta\theta_\alpha + (1-\eta)\theta_\beta = \eta_\alpha\theta_\alpha + \eta_\beta\theta_\beta \tag{14}$$

The double porosity model then describes the transport of moisture by two coupled equations which, in the one dimensional case, are given by

$$\begin{aligned} \eta_\alpha\frac{\partial\theta_\alpha}{\partial t} &= \frac{\partial}{\partial z}\left(\eta_\alpha D_\alpha\frac{\partial\theta_\alpha}{\partial z}\right) - \dot{m} \\ \eta_\beta\frac{\partial\theta_\beta}{\partial t} &= \frac{\partial}{\partial z}\left(\eta_\beta D_\beta\frac{\partial\theta_\beta}{\partial z}\right) + \dot{m} \end{aligned} \tag{15}$$

where $\dot{m}$ describes the exchange of water between the two zones.

This leads to the double permeability model and follows as a natural extension of the double porosity model, namely, by also considering the flow water in the β-zone

$$\begin{aligned} \eta_\alpha \frac{\partial \theta_\alpha}{\partial t} &= \frac{\partial}{\partial z}\left(\eta_\alpha D_\alpha \frac{\partial \theta_\alpha}{\partial z}\right) - \dot{m} \\ \eta_\beta \frac{\partial \theta_\beta}{\partial t} &= \frac{\partial}{\partial z}\left(\eta_\beta D_\beta \frac{\partial \theta_\beta}{\partial z}\right) + \dot{m} \end{aligned} \tag{16}$$

Clearly, these models both reduce to the single continuum model when $\eta_\alpha = 1$, i.e. when the volume fraction of the β-zone is equal to zero.

Besides determining the diffusivities in the two zones, the major problem consists of formulating appropriate mass exchange terms $\dot{m}$. Basically, this term must be determined experimentally. In the following, however, we assume it to be of the type

$$\dot{m} = \omega\left(\frac{\theta_\alpha}{\theta_\alpha^{\max}} - \frac{\theta_\beta}{\theta_\beta^{\max}}\right) \tag{17}$$

where $\theta_\alpha^{\max}$ and $\theta_\beta^{\max}$ are the maximum attainable moisture contents in the two zones and ω is a parameter which governs the rate of mass transfer. This parameter should probably depend on the moisture content in the two zones in a way similar to what is the case with the effective diffusivity. However, for the time being we will assumed it to be constant.

An alternative formulation of the mass exchange term uses the capillary pressures in the two zones, such that

$$\dot{m} = \omega_c\left[p_c^\alpha(S_\alpha) - p_c^\beta(S_\beta)\right] \tag{18}$$

where $p_c{}^\alpha$ and $p_c{}^\beta$ are the capillary pressures, and S_α and S_β are the saturations, or effective saturations, in the two zones. Since fluid flow is driven by differences in pressure rather in than saturation or moisture content, this form of the mass transfer term could be argued as being physically more correct. It does, however, require knowledge of the capillary pressure-saturation curves in the two zones, which naturally increases the complexity of the model. In fact, the departure from the consistent Darcian model of Eq. 8 was motivated by the difficulties involved with the determination of these values. In the following, therefore, we will only consider the moisture content driven mass exchange term (Eq. 17).

For moisture transfer below the fiber saturation point a similar mass exchange term is necessary in order to account for the exchange of water between the vapour found in the lumens and the bound water present in the cell walls. In Krabbenhoft and Damkilde (2003) and Krabbenhoft (2003) it is shown that this should depend on two quantities: the absolute bound water moisture content and some measure of the proximity to equilibrium, such that inter-phase mass exchange decreases dramatically as equilibrium is approached, i.e. much more than can be captured by a first-order expression with constant coefficients such as (Eq. 17). In the case of free water exchange between different zones a similar dependence thus seems worth considering.

Multiple porosity and permeability models

The double porosity and permeability models presented in the previous section are readily extended to include multiple zones. For example, in the case where three zones are present a relevant model could be

$$\begin{aligned}\eta_\alpha \frac{\partial \theta_\alpha}{\partial t} &= \frac{\partial}{\partial z}\left(\eta_1 D_\alpha \frac{\partial \theta_\alpha}{\partial z}\right) - \dot{m}_{\alpha\beta} \\ \eta_\beta \frac{\partial \theta_\beta}{\partial t} &= \frac{\partial}{\partial z}\left(\eta_2 D_\beta \frac{\partial \theta_\beta}{\partial z}\right) + \dot{m}_{\alpha\beta} - \dot{m}_{\beta\gamma} \\ \eta_\gamma \frac{\partial \theta_\gamma}{\partial t} &= \frac{\partial}{\partial z}\left(\eta_3 D_\gamma \frac{\partial \theta_\gamma}{\partial z}\right) + \dot{m}_{\beta\gamma}\end{aligned} \tag{19}$$

where

$$\eta_\alpha + \eta_\beta + \eta_\gamma = 1 \tag{20}$$

In this model exchange of water is assumed to take place between the α and β zones and between the β and γ zones, whereas no exchange takes place between the α and γ zones. Although the complexity of such models increases since more material parameters are required, they may be necessary. Thus, if the results shown in Fig. 5 are to be explained in terms of these models, more than two interacting zones may be required. Here the fractional weight increase curve indicates not only the presence of two, but several different zones.

Examples

In the following, some applications of the models described above are considered. First a set of experimental results is fitted by the double permeability model, after which several different properties of this model are described.

All examples are solved numerically by the finite element method described in the Appendix.

Example 1: Comparison with experimental results

The first example concerns the one dimensional infiltration experiment of fir sapwood (K.K. Hansen and J.B. Jensen, unpublished data) described in Sect. 2 and shown in Fig. 6.

Here the double permeability model was applied with the parameters shown in Table 1. The results in terms of predicted and measured moisture content profiles are shown in Fig. 7, where a dry wood density of 500 kg m^{-3} has been assumed. Even though the fits are not perfect, the results are quite encouraging. The general trend of a rapidly moving fraction with a simultaneous slow absorption is clearly picked up, and a more refined choice of diffusivities could surely lead to a better correspondence between computed and experimental results. The average moisture content as a function of the square root of time is shown in Fig. 8. Again the predicted moisture contents compare quite well to the experimental results.

Table 1 Parameters used in Example 1

Initial moisture content	$\theta_\alpha^0 = \theta_\beta^0 = 55.0\,\mathrm{kg/m^3}$
Maximum moisture content	$\theta_\alpha^{\max} = \theta_\beta^{\max} = 500.0\,\mathrm{kg/m^3}$
Zone fractions	$\eta_{\alpha=0.45}$, $\eta_{\beta=0.55}$
Diffusivities	$D_\alpha = 39.2\times 10^{-9} \exp(0.011\theta_\alpha)$ [m^2/s]
	$D_\beta = 0.0005 D_\alpha$
Mass exchange parameter	$\omega = 55.0\times 10^{-6}\ s^{-1}$

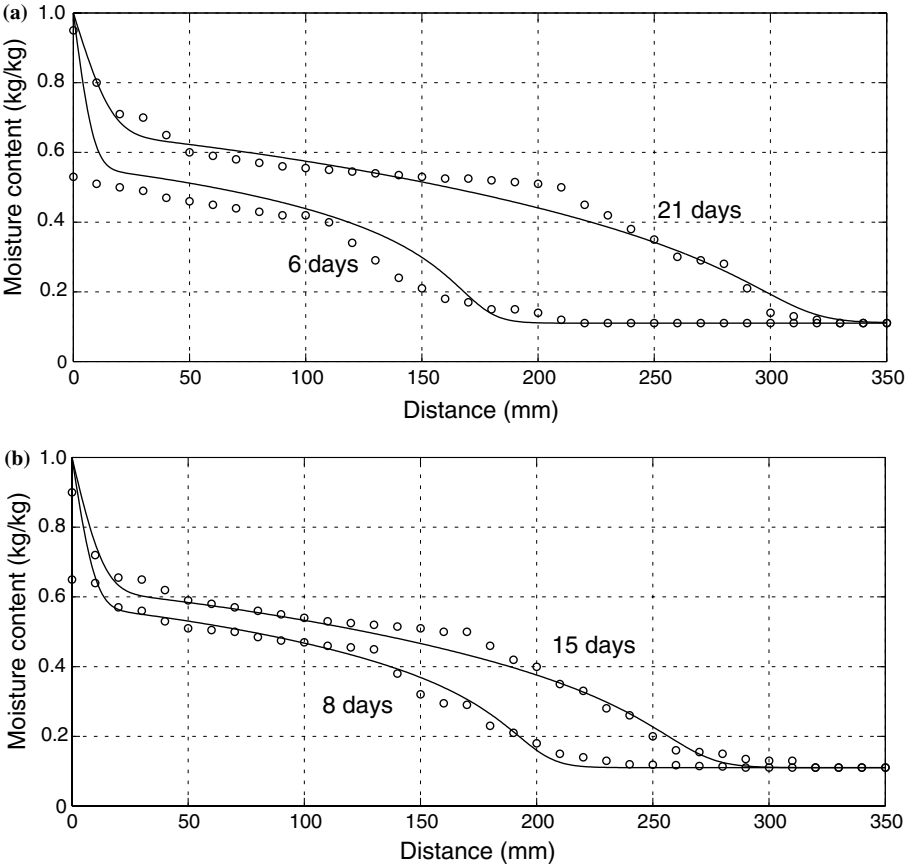

Fig. 7 Computed (-) and experimental (O) moisture profiles. Example 1

Example 2: Double permeability versus double porosity

Since the double porosity model is significantly simpler than the double permeability model in that only one diffusivity is required, it is of interest to compare the results produced by the two models. This is done in Fig. 9a–c. Except for the β-diffusivity all material parameters are identical to the ones used in the previous example.

In Fig. 9a the double permeability model used in the previous example is compared to the double porosity model and, as can be seen, there is a rather good agreement; only very close to the wet end do the models produce significantly different results. In Fig. 9b the β-diffusivity has been increased by a factor of ten and the results deviate slightly more. Finally in Fig. 9, where yet another factor of ten increase is applied, the two models produce quite different results.

Example 3: Sample length dependence

An often reported anomaly is an apparent sample length dependence of the transfer parameters (see e.g. Dinwoodie 1981; Siau 1984; Banks 1981). This

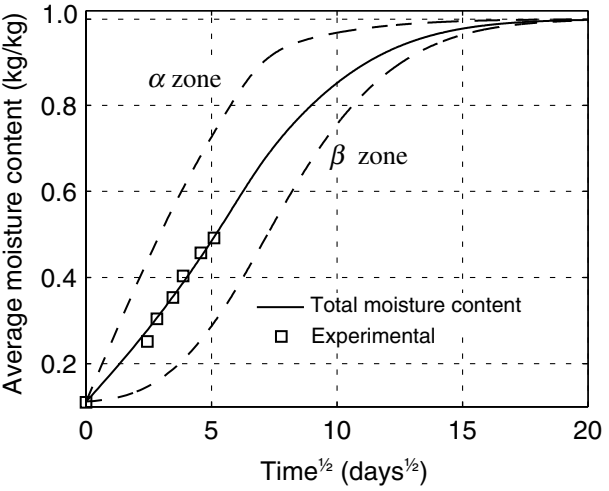

Fig. 8 Average moisture content as a function of square root of time. Example 1

phenomenon is usually attributed to the fact that between the cells, there is a probability of connectivity less than one. This may result in the measured permeabilities being significantly higher for smaller samples than for larger ones. However, the double permeability model results in a manifestation of the opposite phenomenon, namely, that the apparent diffusivity increases with increasing sample dimensions. This is due to non-equilibrium between the water in the two zones as expressed by the mass exchange term $\dot{m}$, and in this sense the situation is identical to what is experienced in moisture transfer below the fiber saturation point (Krabbenhoft and Damkilde 2003). Thus, it can be expected that there are two opposing mechanisms, which naturally complicates matters further.

From classical diffusion theory (see e.g. Crank 1967), it is well known that when the fractional weight increase is plotted as a square root of time divided by the sample length, then the resulting curves should be superimposed on one another. Furthermore, an apparent diffusivity may be computed as

$$\mathrm{D}_{\mathrm{app}} = \frac{\pi a^2}{4}\left(\frac{\mathrm{d}E}{\mathrm{d}\sqrt{t}}\right)^2 \tag{21}$$

where E is the fractional weight increase and a is the sample length (sample half-length if the experiment is conducted with infiltration from both ends), and the slope $\mathrm{d}E/\mathrm{d}\sqrt{t}$ refers to the initial slope of the $E-\sqrt{t}$ curve. However, as discussed previously, in true single continuum diffusion with diffusivity increasing with moisture content the $E-\sqrt{t}$ curve is linear up to around $E\simeq 0.8$, and the slope may then be taken in any point between $E=0$ and $E\simeq 0.8$.

In Fig. 10a, fractional weight increase curves as a function of $\sqrt{t}/a$ are shown for samples of different length for the data set in Table 1. These curves are seen to be far from superimposed on one another. The greatest anomaly occurs for the shorter samples where the α-diffusion quickly comes to an end, and mass exchange between the two zones then takes over and accounts for the larger

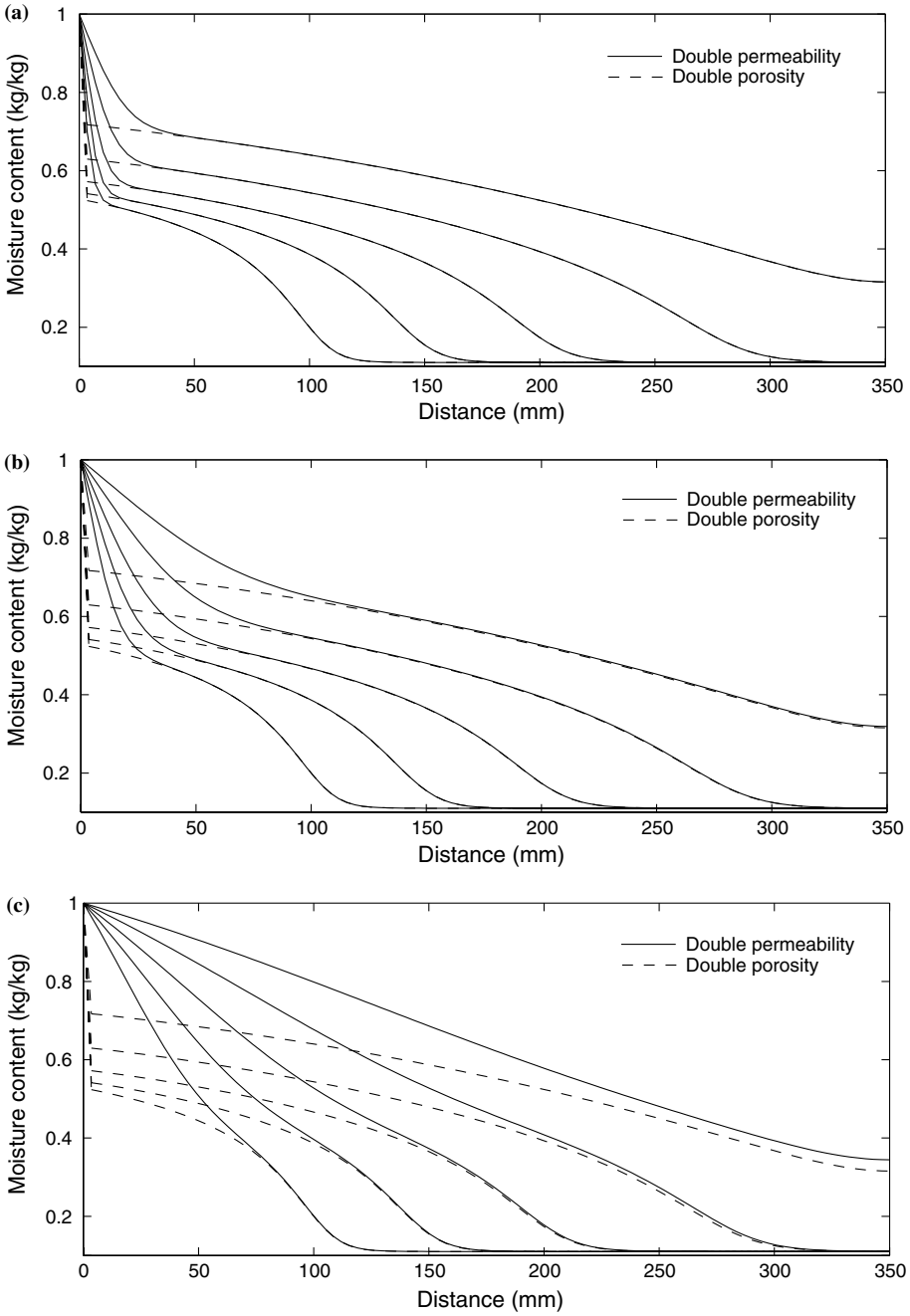

Fig. 9 Dual porosity and permeability models in one dimensional infiltration. Profiles shown after 2, 4, 8, 16, and 32 days. Example 2

part of the remaining uptake of water. The two-stage sorption which results from this becomes less apparent as the length is increased since diffusion then becomes the limiting mechanism.

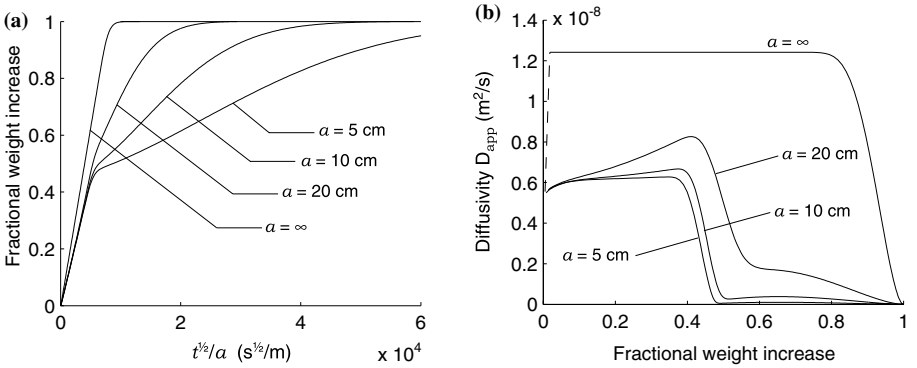

Fig. 10 Fractional weight increase curves (**a**) and apparent diffusivities (**b**). Example 3

In Fig. 10b the apparent diffusivities corresponding to the fractional weight increase curves are shown. These are shown as a function of the fractional weight increase, where at each point the slopes of the $E-\sqrt{t}$ curves have been used. As can be seen, it is only for very large sample lengths, in the order of several meters, that the $E-\sqrt{t}$ curve is perfectly linear and thus gives constant diffusivities up to a point around $E=0.8$ where Eq. 21 is no longer valid. This illustrates the fact that even though the fractional weight increase curve for a sample of $a=20$ cm appears to comply rather well with standard diffusion, the resulting computed diffusivity does not.

Conclusions

In this paper some of the possibilities of applying double porosity and permeability models to the problem of water infiltration into wood have been discussed. Whereas it seems that there is some justification of such models, the problem of determining the necessary material parameters still remains. For this purpose it would seem that determination of moisture profiles would be necessary, or in any case, a great help. Thus, the common total weight increase experiments have been shown to be somewhat problematic in that results which appear to comply rather well with the single continuum diffusion model may in fact be highly anomalous. However, the total weight increase experiment may be useful as a preliminary examination of the qualitative nature of the process, especially if conducted for several samples of different lengths. In this work the total diffusion model which is applicable only for partially saturated conditions and which neglects the effects of gravity has been used. Clearly, this model is not satisfactory, and the consistent Darcian model with water pressure as the driving force should generally be preferred.

Acknowledgements This work has been funded in part by the Danish Research Agency under Project No. 9901363: [no tag]Modeling the Effects of Moisture and Load History on the Mechanical Properties of Wood'. The financial support is gratefully acknowledged.

Appendix

Numerical solution procedure

The numerical solution procedure is described with reference to the double permeability model

$$\begin{aligned} \eta_\alpha \frac{\partial \theta_\alpha}{\partial t} &= \frac{\partial}{\partial z}\left(\eta_\alpha D_\alpha \frac{\partial \theta_\alpha}{\partial z}\right) - \omega\left(\theta_\alpha/\theta_\alpha^{\max} - \theta_\beta/\theta_\beta^{\max}\right) \\ \eta_\beta \frac{\partial \theta_\beta}{\partial t} &= \frac{\partial}{\partial z}\left(\eta_\beta D_\beta \frac{\partial \theta_\beta}{\partial z}\right) + \omega\left(\theta_\alpha/\theta_\alpha^{\max} - \theta_\beta/\theta_\beta^{\max}\right) \end{aligned} \tag{22}$$

The moisture content variables are approximated in terms of finite element functions as

$$\begin{aligned} \theta_\alpha(z,t) &\approx \mathbf{N}(z)\theta_\alpha(t) \\ \theta_\beta(z,t) &\approx \mathbf{N}(z)\theta_\beta(t) \end{aligned} \tag{23}$$

Similarly, the diffusivities are approximated in terms of their nodal values

$$\begin{aligned} D_\alpha &= \mathrm{A}\mathbf{D}_\alpha \\ D_\beta &= \mathrm{A}\mathbf{D}_\beta \end{aligned} \tag{24}$$

where the vectors $\mathbf{D}_\alpha = D_\alpha\,(\theta_\alpha)$ and $\mathbf{D}_\beta = D_\beta\,(\theta_\beta)$ contain the nodal diffusivities and $\mathbf{A}$ is a vector which weights these in an appropriate way as being representative for the element. In all the examples presented $\mathbf{A} = \left[\frac{1}{2}, \frac{1}{2}\right]$. Alternative upstream weighting schemes are discussed in Forsyth and Kropinski (1997).

Applying the standard Galerkin scheme (see e.g. Zienkiewicz and Taylor 2000) to Eq. 22 yields two coupled nonlinear ordinary differential equations

$$\begin{aligned} \mathrm{r}_\alpha &= \eta_\alpha \mathbf{M}\frac{\mathrm{d}\theta_\alpha}{\mathrm{d}t} + \mathbf{K}\theta_\alpha + \tilde{\omega}_\alpha \mathbf{M}\theta_\alpha - \tilde{\omega}_\beta \mathbf{M}\theta_\beta = \mathbf{0} \\ \mathrm{r}_\beta &= \eta_\beta \mathbf{M}\frac{\mathrm{d}\theta_\beta}{\mathrm{d}t} + \mathbf{K}\theta_\beta + \tilde{\omega}_\alpha \mathbf{M}\theta_\alpha + \tilde{\omega}_\beta \mathbf{M}\theta_\beta = \mathbf{0} \end{aligned} \tag{25}$$

where $\tilde{\omega}_\alpha = \omega/\theta_\alpha^{\max}$ and $\tilde{\omega}_\beta = \omega/\theta_\beta^{\max}$. Assuming $\mathbf{A}$ is constant, the matrices $\mathbf{M}$, $\mathbf{K}_\alpha$ and $\mathbf{K}_\beta$ are given by

$$\mathbf{M} = \int_\Omega \mathbf{N}^{\mathrm{T}}\mathbf{N}\mathrm{d}\Omega \tag{26}$$

$$\mathbf{K}_\alpha = \tilde{\mathbf{K}}\mathrm{A}\mathbf{D}_\alpha, \quad \mathbf{K}_\beta = \tilde{\mathbf{K}}\mathrm{A}\mathbf{D}_\beta \tag{27}$$

where

$$\tilde{\mathbf{K}} = \int_\Omega \left(\frac{\partial \mathbf{N}}{\partial z}\right)^{\mathrm{T}} \frac{\partial \mathbf{N}}{\partial z}\mathrm{d}\Omega \tag{28}$$

It should be noted that in practice $\mathbf{M}$ is replaced with a lumped equivalent in order to reduce the risk of non-physical oscillations (see e.g. Segerlind 1984).

The backward Euler scheme is now applied whereby the fully discretized equations can be written as

$$\begin{aligned}\mathbf{r}_\alpha &= \left[(\eta_\alpha + \tilde{\omega}_\alpha \Delta t)\mathbf{M} + \Delta t \mathbf{K}_{\alpha,n+1}\right]\theta_{\alpha,n+1} - \tilde{\omega}_\beta \Delta t \mathbf{M}\theta_{\beta,n+1} - \eta_\alpha \mathbf{M}\theta_{\alpha,n} = \mathbf{0} \\ \mathbf{r}_\beta &= \left[(\eta_\beta + \tilde{\omega}_\beta \Delta t)\mathbf{M} + \Delta t \mathbf{K}_{\beta,n+1}\right]\theta_{\beta,n+1} - \tilde{\omega}_\alpha \Delta t \mathbf{M}\theta_{\alpha,n+1} - \eta_\beta \mathbf{M}\theta_{\beta,n} = \mathbf{0}\end{aligned} \tag{29}$$

where subscript n refers to the current state and $n+1$ to the new unknown state. Due to the nonlinearity contained in $\mathbf{K}_\alpha$ and $\mathbf{K}_\beta$ an iterative procedure is applied. If the standard Newton-Raphson scheme is applied, increments $\Delta\theta_\alpha$ and $\Delta\theta_\beta$ are computed by solution of the following linear system of equations

$$\begin{bmatrix}\mathbf{J}_{\alpha\alpha} & \mathbf{J}_{\alpha\beta} \\ \mathbf{J}_{\beta\alpha} & \mathbf{J}_{\beta\beta}\end{bmatrix}^j_{n+1} \begin{bmatrix}\Delta\theta_\alpha \\ \Delta\theta_\beta\end{bmatrix}^j_{n+1} = -\begin{bmatrix}\mathbf{r}_\alpha \\ \mathbf{r}_\beta\end{bmatrix}^j_{n+1} \tag{30}$$

after which the current state is updated as

$$\begin{bmatrix}\theta_\alpha \\ \theta_\beta\end{bmatrix}^{j+1}_{n+1} \begin{bmatrix}\theta_\alpha \\ \theta_\beta\end{bmatrix}^j_{n+1} + \begin{bmatrix}\Delta\theta_\alpha \\ \Delta\theta_\beta\end{bmatrix}^j_{n+1} \tag{31}$$

where the initial point is taken as the last converged, i.e.

$$\begin{bmatrix}\theta_\alpha \\ \theta_\beta\end{bmatrix}^0_{n+1} = \begin{bmatrix}\theta_\alpha \\ \theta_\beta\end{bmatrix}_n \tag{32}$$

The Jacobians in Eq. 30 are given by

$$\begin{aligned}\mathbf{J}_{\alpha\alpha} &= (\eta_\alpha + \tilde{\omega}_\alpha \Delta t)\mathbf{M} + \Delta t(\mathbf{K}_\alpha + \mathbf{K}^g_\alpha) \\ \mathbf{J}_{\beta\beta} &= (\eta_\beta + \tilde{\omega}_\beta \Delta t)\mathbf{M} + \Delta t(\mathbf{K}_\beta + \mathbf{K}^g_\beta) \\ \mathbf{J}_{\alpha\beta} &= -\tilde{\omega}_\beta \Delta t \mathbf{M} \\ \mathbf{J}_{\beta\alpha} &= -\tilde{\omega}_\alpha \Delta t \mathbf{M}\end{aligned} \tag{33}$$

where

$$\mathbf{K}^g_\alpha = \tilde{\mathbf{K}}\theta_\alpha \mathbf{A}\left[\frac{\partial \mathbf{D}_\alpha}{\partial \theta_\alpha}\right], \quad \mathbf{K}^g_\beta = \tilde{\mathbf{K}}\theta_\beta \mathbf{A}\left[\frac{\partial \mathbf{D}_\beta}{\partial \theta_\beta}\right] \tag{34}$$

These matrices are unsymmetric and are, for this reason, often left out. Although this does influence the convergence rate in a negative way, it may lead to smaller total cpu times as compared to the full Newton scheme (see Paniconi and Putti 1994).

References

Banks WB (1981) Addressing the problem of non-steady state liquid flow in wood. Wood Sci Technol 15:171–177

Couture F, Jomaa W, Puiggali JR (1996) Relative permeability relations: a key factor for a drying model. Transport Porous Med 23:303–335

Crank J (1967) The mathematics of diffusion. Oxford University Press, Oxford

Dinwoodie JM (1981) Timber, its nature and behaviour. Van Norstrand Reinhold, New York

Forsyth PA, Kropinski MC (1997) Monotonicity considerations for saturated-unsaturated subsurface flow. SIAM J Sci Comput 18:1328–1354

Goyeneche M, Lasseux D, Bruneau D (2002) A film-flow model to describe free water transport during drying of a hygroscopic capillary porous medium. Transport Porous Med 48:125–158

Hansen MH (1993) Estimation of transfer coefficients in models for coupled heat and moisture transfer in porous media. PhD Thesis, Technical University of Denmark, Lyngby

Haria HA, Hodnett MG, Johnson AC (2003) Mechanisms of groundwater recharge and pesticide penetration to a chalk aquifer in southern England. J Hydrol 275:122–137
Krabbenhoft K (2003) Transport phenomena in wood. PhD Thesis, Technical University of Denmark, Lyngby
Krabbenhoft K, Damkilde L (2003) A non-equilibrium model for non-Fickian moisture transfer in wood. Mater Struct (In press)
Krabbenhoft K, Bechgaard C, Damkilde L, Hoffmeyer P (2003) Finite element analysis of boron diffusion in wooden poles. In: Jarmer J (ed) Proceedings of the 34th annual conference of the international research group on wood preservation, Stockholm, pp 1–14
Krus M, Hansen KK, Küntzel HM (1997) Porosity and liquid absorption of cement paste. Mater Struct 40:394–398
Kuntz M, Lavallee P (2001) Experimental evidence and theoretical analysis of anomalous diffusion during water infiltration in porous building materials. J Phys D Appl Phys 34:2547–2554
Lewis RW, Schrefler BA (2000) The finite element method in the static and dynamic deformation and consolidation of porous media, 2nd edn. Wiley, New York
Lockington DA, Parlange JY (2003) Anomalous water absorption in porous materials. J Phys D Appl Phys 36:760–767
Martys NS, Ferraris CF (1997) Capillary transport in mortars and concrete. Cement Concrete Res 27:747–760
Mortensen AP (2001) Preferential flow phenomena in partially-saturated porous media. PhD Thesis, Enviroment and Resources, Technical University of Denmark, Lyngby
Nielsen AF (1974) Moisture distributions in cellular concrete during heat and moisture transfer. PhD Thesis, Technical University of Denmark, Lyngby
Ouelhazi N, Arnaud G, Fohr JP (1992) A two-dimensional study of wood plank drying. The effect of gaseous pressure below boiling point. Transport Porous Med 7(1):39–61
Pang S (1998) Relative importance of vapour diffusion and convective flow in modelling of softwood drying. Dry Technol 16:271–281
Paniconi C, Putti M (1994) A comparison of Picard and Newton iteration in the numerical solution of multidimensional variably saturated flow. Water Resour Res 30:3357–3374
Pel L (1995) Moisture transport in porous building materials. PhD Thesis, Technical University Eindhoven, The Netherlands
Perre P (1987) Measurements of softwoods' permeability to air: importance upon the drying model. Int Commun Heat Mass 14:519–529
Perre P (1998) The use of homogenization to simulate heat and mass transfer in wood: towards a double porosity approach. In: Drying '98—Proceedings of the international drying symposium, vol A, Halkidiki, pp 57–72
Perré P, Turner IW (1999) A 3-D version of TransPore: a comprehensive heat and mass transfer computational model for simulating the drying of porous media. Int J Heat Mass Tran 42:4501–4521
Perre P, Turner IW (1999) Transpore: a generic heat and mass transfer computational model for understanding and visualising the drying of porous media. Dry Technol 17(7–8):1273–1289
Segerlind LJ (1984) Applied finite element analysis, 2nd edn. Wiley, New York
Siau JF (1984) Transport processes in wood. Springer, Berlin Heidelberg New York
Signe Kamp J (2003) Drying of wood. PhD Thesis, Technical University of Denmark, Lyngby
Structure of Wood (2003) Society of Wood Science and Technology, Teaching Unit No. 1, http://www.swst.org/teach/set2/struct1.html. Cited 16 June 2003
Spolek GA, Plumb OA, Olmstead BA (1985) Heat and mass transfer in wood during drying. Int J Heat Mass Tran 28(9):1669–1678
Tremblay C, Cloutier A, Fortin Y (2000) Determination of the effective water conductivity of red pine sapwood. Wood Sci Technol 34:109–124
Wadsö L (1994) Describing non-Fickian water-vapour sorption in wood. J Mater Sci 29:2367–2372
Whitaker S (1977) Simultaneous heat, mass, and momentum transfer in porous media: a theory of drying. Adv Heat Transfer 13:119–203
Zienkiewicz OC, Taylor RL (2000) The finite element method. Butterworth-Heinemann, Oxford